DIRECT LASER WRITING OF TRIANGULAR-WALLED MICROARRAYS ONTO GLASS DIFFUSERS TO ENABLE CONTROLLED REFLECTIVITY UNDER ADAPTIVE OPTICS OPHTHALMIC IMAGING SYSTEMS

Ian Rosenthal[1,2], Lucas Garcia-O'Donnell[1], Brian Ngoh[1], Zhuolin Liu[2], Daniel X. Hammer[2], Anant Agrawal[2], and Ryan D. Sochol[1]
[1]University of Maryland, College Park, MD, USA
[2]U.S. Food and Drug Administration, Silver Spring, MD, USA

ABSTRACT

Adaptive optics scanning laser ophthalmoscopy (AOSLO) is an emerging imaging modality capable of resolving photoreceptors and microscopic structures in the living human retina, allowing clinicians to non-invasively detect retinal pathologies unseen by other methods. Widespread clinical use of complex imaging systems like AOSLO often requires standardized system performance assessments with "phantoms"—accurate physical models of anatomical structures. To date, however, challenges in manufacturing retinal phantoms at relevant scales has hindered such standardization for AOSLO. To overcome these barriers, here we introduce novel microwell array phantoms that comprise triangular sidewalls—enabled by the submicron-scale geometric versatility of "Direct Laser Writing (DLW)"-based additive manufacturing—and are 3D printed directly onto glass diffusers. The array geometries mimic retinal photoreceptor mosaic attributes (cell diameter and spacing) and are combined with a glass diffuser surface texture, which allows for high control over reflectivity, critical for informative AOSLO image capture. Experimental AOSLO imaging results revealed peak-to-valley grayscale differentiation of 160±25.4 and 190±29.6 (a.u.) for the 5 μm and 9 μm center-to-center arrays, respectively, suggesting attainment of phantom performance pertinent to the evaluation of AOSLO spatial resolution. Thus, the concepts presented here establish a pathway for new classes of AOSLO phantoms to support greater clinical use.

KEYWORDS

Adaptive Optics, Additive Manufacturing, 3D Printing, Direct Laser Writing, Two-Photon Polymerization, Phantoms

INTRODUCTION

Adaptive optics scanning laser ophthalmoscopy (AOSLO) is uniquely suited for detecting and monitoring retinal diseases by visualization of key retinal cells and structures [1] *via* correction of aberrations present in the human eye [2]. First demonstrated by Liang *et al*., adaptive optics operates with a wavefront sensor to measure the magnitude of ocular aberrations and a deformable mirror to correct the wave aberrations [3]. AOSLO systems can resolve single photoreceptors within their mosaic [4]. Other relevant microscopic structures, including ganglion cells [5], vasculature [6], Henle fibers [7], and retinal pigment epithelial cells, can also be investigated in detail with AOSLO [8]. Despite such promise, concerns regarding the repeatability of optical measurements remain a significant barrier to mainstream clinical adoption of AOSLO systems [9].

Retinal "phantoms"—physical models that recapitulate the structural and optical characteristics of *in vivo* anatomy—offer the potential to address these issues by standardizing AOSLO system performance assessment to minimize undesired clinical variability [10]. Unfortunately, manufacturing photoreceptor mosaic phantoms at biologically relevant scales without compromising reflectivity performance has remained a critical challenge. For example, micropost array-based phantoms produce irregular patterns and require protocols that increase the potential for undesired variations [11, 12]. Notably, the micropost structure contributes to anti-reflectivity properties that reduce the phantom capabilities as the arrays at spacings expected to be resolved appear as dark regions [13]. Recent advances in the two-photon (or multi-photon) additive manufacturing strategy, "Direct Laser Writing (DLW)", provides distinctive benefits for fabricating retinal phantoms at accurate length scales and with unparalleled freedom in geometric design [14-16]. By harnessing this technology, here we shift away from established micropost array-based approaches to instead investigate novel DLW-enabled microwell array phantoms with triangular sidewalls that are 3D printed directly onto glass diffuser substrates.

CONCEPT

The overall concept for DLW-based 3D printing of triangular-walled microwell arrays onto a glass diffuser (which comprises a random surface texture) for the optics community are presented in **Figure 1**. The diffuser is mounted in a DLW 3D printer where the roughened surface—immersed in a photocurable material—is aligned with the objective lens (**Fig. 1a**). Importantly, in contrast to prior work in which phantoms were manufactured onto smooth substrates [17], the decision to print the phantom atop the relatively rough texture of the glass diffuser is motivated by the capacity for such surfaces to yield uniform light distribution in the wavefront sensor image for stable adaptive optics correction. Next, a 3D

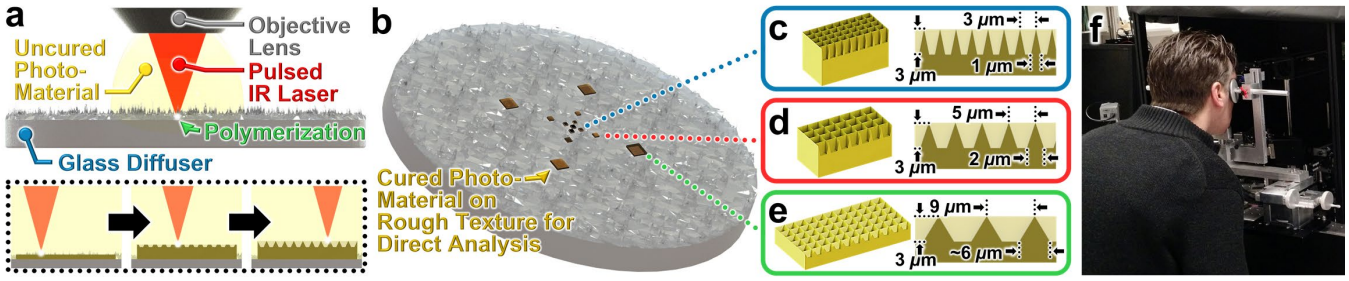

***Figure 1**: Concept of "Direct Laser Writing (DLW)"-based triangular-walled retinal phantoms for Adaptive Optics Scanning Light Ophthalmoscopy (AOSLO). **(a, b)** Concept of DLW-print microwell arrays onto a glass diffuser. **(c–e)** Cross sections of **(c)** 3 μm, **(d)** 5 μm, and **(e)** 9 μm center-to-center designs. **(f)** Example of AOSLO imaging a human subject.*

978-1-940470-04-7/HH2022/$25©2022TRF
DOI 10.31438/trf.hh2022.75

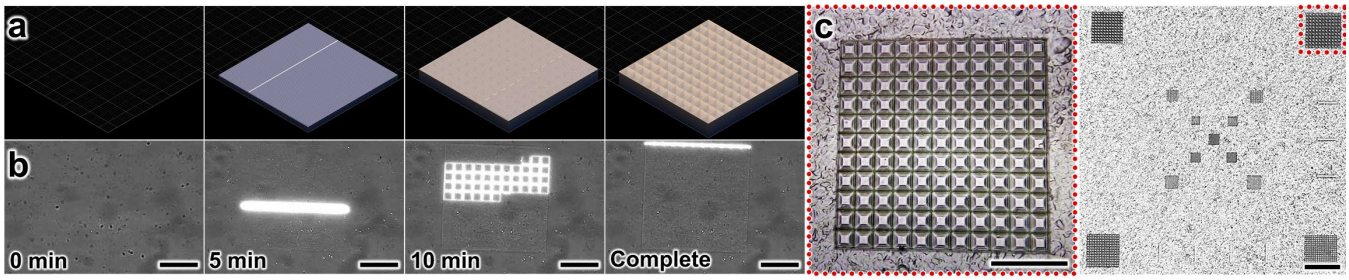

***Figure 2**: Sequential images of **(a)** simulations, and **(b)** the corresponding DLW printing process for a representative array. Scale bars = 20 µm. **(c)** Brightfield of the retinal phantom comprising multiple, distinct arrays (highlighting the 9 µm array). Scale bar = 20 µm; Expanded view scale bar = 100 µm.*

microwell array is printed directly onto the diffuse surface by scanning a femtosecond pulsed infrared (IR) laser point-by-point, layer-by-layer, to induce polymerization of the photomaterial in target locations (**Fig. 1a – *inset***). The glass diffuser-structure assembly is removed from the DLW printer and placed in a developer solution to remove any uncured photomaterial, leaving the microwell array adhered to the surface of the glass diffuser (**Fig. 1b**). Due to the geometric control and submicron feature resolution afforded by the DLW technology, each triangular-walled microwell array can be designed with distinct dimensions (*e.g.*, **Fig. 1c–e**) that are relevant to AOSLO imaging of the human retina (**Fig. 1f**).

MATERIALS AND METHODS

DLW-Printing of 3D Microwell Structures

All DLW protocols in this work are based on the use of a Nanoscribe Photonic Professional GT2 DLW 3D printer (Nanoscribe GmbH, Karlsruhe, Germany). Prior to printing, borosilicate ground glass diffusers (DG10-1500, Thorlabs, Inc., Newton, NJ), with a thickness of 2 mm and a diameter of 25.4 mm, were washed and rinsed with acetone and isopropyl alcohol (IPA). Once dried, the surface designated for print adhesion was placed face-up in a tabletop Plasma Cleaner (PIE Scientific, Union City, CA) and exposed to Oxygen plasma for 30 minutes. Once the cycle was complete, the substrate was placed in a bath of ethanol/3-(trimethoxysilyl)propyl methacrylate solution for 1 hour. The substrate was removed from the solution, rinsed with acetone and DI water, and dried. Then, the glass diffuser was mounted into the Nanoscribe DLW printer with a single droplet of IP-Dip2 photoresist (Nanoscribe). The substrate is mounted in the "Dip-in Laser Lithography (DiLL)" configuration, with the lens immersed in the photoresist.

The computer-aided design (CAD) software, SolidWorks (Dassault Systèmes, France), was used to generate 3D models of the triangular-walled microwell arrays with varying center-to-center distances. These distances were selected to mimic photoreceptor mosaics of the human eye across the macula at different retinal eccentricities to evaluate the resolution capabilities of AOSLO systems for clinical use. Each model was exported as an STL file and then imported into the computer-aided manufacturing (CAM) software, Describe (Nanoscribe), for laser writing path generation. All designs included 100 nm hatching and 100 nm layer heights with 2 contours spaced 100 nm apart.

All designs were printed with the 63× objective lens in DiLL mode with a laser power of 35 mW and a laser scanning speed of 25 mm/s. Due to the abnormal surface texture and to account for any unintended deviations, the surface interface of the glass diffuser was found manually. The DLW printing process was initiated with approximately 3 µm of overlap into the glass (with respect to the surface interface). Following the DLW process, the diffuser-print

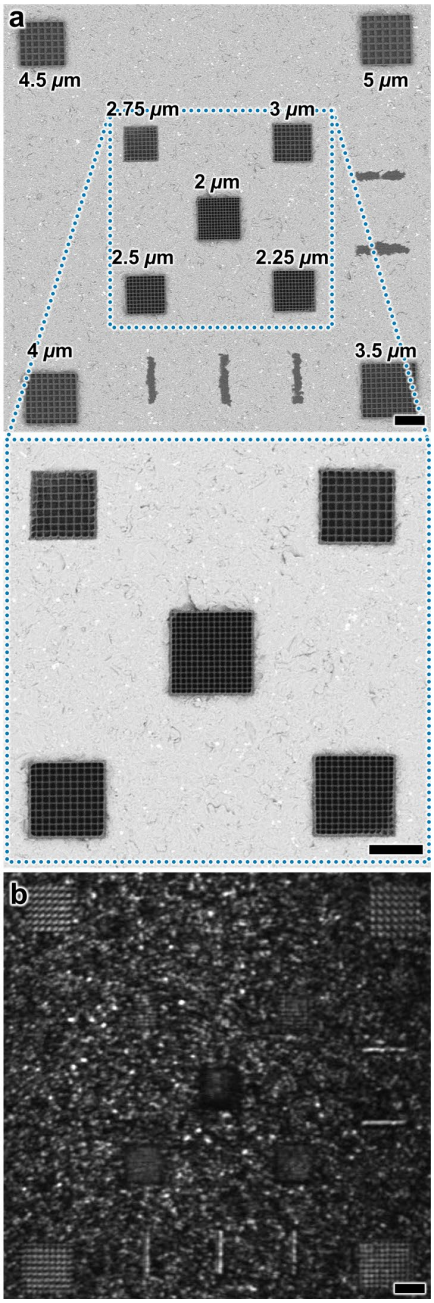

***Figure 3**: Fabrication results. **(a)** SEM micrographs of 2–5 µm triangular-walled microwell arrays. **(b)** A corresponding AOSLO image of the 2–5 µm arrays. Scale bar = 20 µm.*

assembly was removed from the printer, developed using propylene glycol methyl ether acetate (PGMEA) for 20 min, and then IPA for 5 min. The assembly was dried using Nitrogen gas.

Phantom Characterization

Scanning electron microscope (SEM) images of the DLW-based prints were captured using a Phenom XL G2 Benchtop SEM (Thermo Fisher Scientific, Waltham, MA). AOSLO images were captured using an AOSLO system that was custom-built in the FDA laboratory for investigational use on human subjects [18]. For AOSLO imaging, the phantoms were placed at the retinal plane of a model eye, which uses an achromatic glass lens to replicate the focusing properties of a typical human eye. The model eye assembly includes a translation mount for the phantom to bring the printed structures into the center of the AOSLO field of view. Quantitative analysis of AOSLO images was performed with ImageJ (NIH, Bethesda, MD) to determine reflectivity and spatial dimensions *via* established methods [19].

RESULTS AND DISCUSSION

CAM simulations and corresponding micrographs of the DLW-based 3D printing process for a representative microwell array (*i.e.*, the 9 μm center-to-center design) are presented in **Figure 2a** and **2b**, respectively. The entire printing process for each print field (~140×140 μm^2) was completed in less than 15 min. Larger arrays such as the 9 μm array (side length = 99 μm) occupied an entire print field, while arrays with smaller center-to-center distances and side lengths less than 30 μm, such as the 2–3 μm designs, could be included in a single print field, reducing the total print time. Fabrication results revealed effective DLW-based printing fidelity for all the microwell array designs examined despite the non-uniformity of the glass diffuser's rough surface (**Fig. 2c**; **Fig. 3a**).

AOSLO images of the phantom exhibited distinct bright spots in patterns corresponding directly to the microwell arrays (**Fig. 3**)—a critical requirement for imaging characterization. The AOSLO results revealed two key trends. First, the arrays with ≤3 μm center-to-center spacings could not be resolved, and therefore, clearly set a meaningful resolution performance limit for AOSLO (*e.g.*, **Fig. 4a,d**). For example, quantified AOSLO grayscale intensities for the 3 μm design revealed indistinguishable peak-to-valley results (**Fig. 4g**). In contrast, we observed that the larger spacing-associated designs were not only directly visible, but that the imaging conspicuity improved further with increasing center-to-center spacing. For example, the quantified AOSLO peak-to-valley grayscale results increased from 160±25.4 to 190±29.6 (a.u.) for the 5 μm and 9 μm cases, respectively (**Fig. 4**).

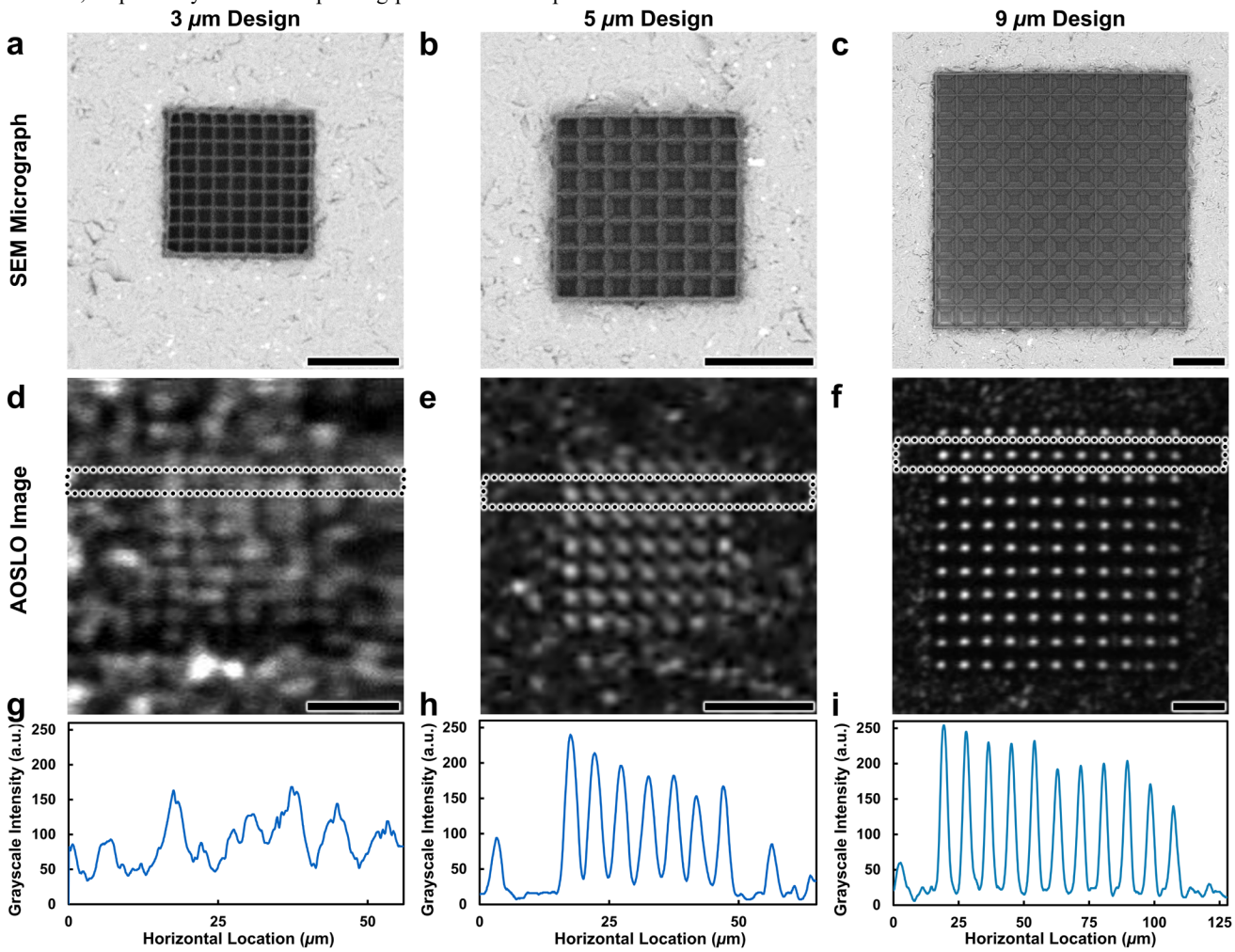

***Figure 4**: Imaging results for the microwell array design. **(a–c)** SEM micrographs, **(d–f)** Corresponding AOSLO images, and **(g–i)** Quantified gray-scale intensities along a representative region of interest of the AOSLO images for microwell arrays with center-to-center designs of: **(a, d, g)** 3 μm, **(b, e, h)** 5 μm, and **(c, f, i)** 9 μm designs. Scale bars = 20 μm.*

CONCLUSIONS

In this work, we investigated a novel strategy for using DLW-based additive manufacturing to 3D print triangular-walled microwell structures directly onto glass diffusers. Previous retinal phantoms from our group required intensive fabrication strategies to achieve an effective phantom including encapsulating gold-coated, micropost structures in PDMS and placing that assembly behind an IPA-filled chamber for index matching within the model eye [11]. Such a complex setup hindered adoption by the AOSLO research community, thus limiting the impact. Later work by our group included a micropost-based system that was limited by irregular reflection patterns from the interstitial space that reduced functionality [12, 19]. Furthermore, previous phantoms used diffuse textures printed on the smooth side of a Si wafer, which led to additional molding strategies and increased fabrication time. In contrast, the fabrication strategy presented here achieved effective photoresist-to-substrate bonding, enabling immediate AOSLO imaging following development. AOSLO imaging demonstrated patterned reflectivity based on varied center-to-center distances. Additional design modifications could further enhance the visibility of the arrays in relation to the adjacent diffuse texture and improve the integrity of the overall structure. Future experiments will investigate phantom-to-phantom repeatability and sources of variation among manufactured microwell arrays, especially for smaller center-to-center distance designs. Overall, these results serve as a fundamental proof of concept of the triangular-walled microwell array phantom as a means to efficiently compare and track AOSLO system performance.

ACKNOWLEDGEMENTS

We greatly appreciate the contributions of Olivia M. Young, Ziteng Wen, Robert Propst, the members of the Bioinspired Advanced Manufacturing (BAM) laboratory and Terrapin Works staff at the University of Maryland, College Park. This research was supported in part by U.S. National Science Foundation (NSF) Award #1943356. Ian Rosenthal was supported by the Oak Ridge Institute for Science and Engineering (ORISE) fellowship program at the FDA.

DISCLAIMER

The mention of commercial products, their sources, or their use in connection with material reported herein is not to be construed as either an actual or implied endorsement of such products by the U.S. Department of Health and Human Services.

REFERENCES

[1] M. Georgiou, A. Kalitzeos, E. J. Patterson, A. Dubra, J. Carroll, and M. Michaelides, “Adaptive optics imaging of inherited retinal diseases,” *British Journal of Ophthalmology*, 102, 8 (2018) pp. 1028–1035.

[2] A. Roorda, and J. L. Duncan, “Adaptive Optics Ophthalmoscopy,” *Annual Review of Vision Science*, 1 (2015) pp. 19-50.

[3] J. Liang, D. R. Williams, and D. T. Miller, "Supernormal vision and high-resolution retinal imaging through adaptive optics," *J. Opt. Soc. Am. A,* 14 (1997) pp. 2884 - 2892.

[4] K. M. Litts, R. F. Cooper, J. L. Duncan, J. Carroll, “Photoreceptor-Based Biomarkers in AOSLO Retinal Imaging,” *Invest. Ophthalmol. Vis. Sci*., 58, 6 (2017) pp. BIO255-BIO267.

[5] L. Yin, B. Masella, D. Dalkara, J. Zhang, G. Flannery, D. V. Schaffer, D. R. Williams, and W. H. Merigan, “Imaging light responses of foveal ganglion cells in the living macaque eye,” *The Journal of Neuroscience: the Official Journal of the Society for Neuroscience*, 34, 19 (2014) pp. 6596–6605.

[6] Z. Popovic, P. Knutsson, J. Thaung, M. Owner-Petersen, and J. Sjöstrand, “Noninvasive imaging of human foveal capillary network using dual-conjugate adaptive optics,” *Investigative Ophthalmology & Visual Science*, 52, 5 (2011) pp. 2649–2655.

[7] D. Scoles, B. P. Higgins, R. F. Cooper, A. M. Dubis, P. Summerfelt, D. V. Weinberg, J. E. Kim, K. E. Stepien, J. Carroll, and A. Dubra, “Microscopic Inner Retinal Hyper-Reflective Phenotypes in Retinal and Neurologic Disease,” *Invest. Ophthalmol. Vis. Sci.,* 55, 7 (2014) pp. 4015-4029.

[8] D. Scoles, Y. N. Sulai, and A. Dubra, “In vivo dark-field imaging of the retinal pigment epithelium cell mosaic. *Biomedical Optics Express*, 4, 9 (2013) pp. 1710–1723.

[9] N. Wynne, J. Carroll, and J. L. Duncan, “Promises and pitfalls of evaluating photoreceptor-based retinal disease with adaptive optics scanning light ophthalmoscopy (AOSLO),” *Prog Retin Eye Res*, 83 (2021) pp. 100920.

[10] H. J. Lee, N. M. Samiudin, T. G. Lee, I. Doh, and S. W. Lee, “Retina phantom for the evaluation of optical coherence tomography angiography based on microfluidic channels,” *Biomed Opt Express*, 10, 11 (2019) pp. 5535–5548.

[11] N. Kedia, Z. Liu, R. D. Sochol, J. Tam, D. X. Hammer, and A. Agrawal, “3-D printed photoreceptor phantoms for evaluating lateral resolution of adaptive optics imaging systems,” *Opt. Lett.,* 44, 7 (2019) pp. 1825–1828.

[12] A. C. Lamont, M. A. Restaino, A. T. Alsharhan, Z. Liu, D. X. Hammer, A. Agrawal, and R. D. Sochol, “Direct Laser Writing of Titanium Dioxide-Laden Retinal Cone Phantoms,” *2020 IEEE 33rd International Conference on Micro Electro Mechanical Systems (MEMS)*, (2020) pp. 1223–1226.

[13] I. Zada, W. Zhang, Y. Li, P. Sun, N. Cai, J. Gu, Q. Liu, H. Su, and D. Zhang, "Angle dependent antireflection property of TiO2 inspired by cicada wings," *Appl. Phys. Lett.* 109, 15 (2016).

[14] V. Hahn, P. Kiefer, T. Frenzel, J. Qu, E. Blasco, C. Barner-Kowollik, and M. Wegener, "Rapid Assembly of Small Materials Building Blocks (Voxels) into Large Functional 3D Metamaterials", *Advanced Functional Materials*, 30, 26 (2020) pp. 1907795.

[15] A.C. Lamont, M. Restaino, M. Kim, and R.D. Sochol, "A facile multi-material direct laser writing strategy", *Lab on a Chip*, 19, 14 (2019) pp. 2340-2345.

[16] A.T. Alsharhan, R. Acevedo, R. Warren, and R.D. Sochol, "3D microfluidics *via* cyclic olefin polymer-based *in situ* direct laser writing", *Lab on a Chip*, 19, 17 (2019) pp. 2799-2810.

[17] A. Agrawal, A. C. Lamont, Z. Liu, R. D. Sochol, and D. X. Hammer, “Engineered Texture Phantom for Measuring Lateral Resolution of Adaptive Optics Ophthalmic Imaging Systems,” in *Imaging and Applied Optics Congress* (2020).

[18] Z. Liu, J. Tam, O. Saeedi, and D. X. Hammer, "Trans-retinal cellular imaging with multimodal adaptive optics," *Biomedical Opt. Express,* 9, 9 (2018) pp. 4246-4262.

[19] C. A. Schneider, W. S. Rasband, and K. W. Eliceiri, “NIH Image to ImageJ: 25 years of image analysis,” *Nature Methods*, 9 (2012) pp. 671-675.

CONTACT

* I. Rosenthal, tel: +1 (301) 405-6928; irosenth@terpmail.umd.edu